



Room temperature dielectric and optical studies of Cd-doped ZnO nanostructures

GYANENDRA PRATAP SINGH^{1,*}, ABHAY KUMAR AMAN², RAKESH KUMAR SINGH² and M K ROY¹

¹Department of Natural Science, PDPM Indian Institute of Information Technology Design and Manufacturing Jabalpur, Jabalpur 482005, India

²Aryabhata Centre for Nanoscience and Nanotechnology, Aryabhata Knowledge University, Patna 800001, India

*Author for correspondence (1616602@iiitdmj.ac.in)

MS received 1 October 2020; accepted 28 January 2021

Abstract. In the current investigation, we report successful synthesis of well-crystalline Cd-doped ZnO nanostructures above their miscibility range ($Zn_{1-x}Cd_xO$, $x = 0.1, 0.2, 0.3,$ and 0.4) via an easy and simple low-temperature solution method. The as-prepared samples were studied for their structural, optical and electrical behaviour as a function of Cd doping. The X-ray diffraction reveals that the as-prepared samples possess a pure hexagonal wurtzite structure of ZnO without any essence formation of a separate CdO phase up to 30% of Cd doping. However, on increasing the Cd concentration i.e., > 30%, clustering of CdO (as a separate phase) is visible in X-ray pattern. Ultraviolet–visible (UV–Vis) spectra show the effective change in the optical band gap with increase in Cd doping. Zn–O stretching modes of vibrations are confirmed by Fourier transform infrared spectroscopy in all samples. The frequency-dependence behaviour of dielectric constant, dielectric loss and ac conductivity of as-prepared samples were studied at room temperature. The colossal dielectric response is found to be $\sim 6 \times 10^3$ at 1 kHz for Cd-doped samples. The observed dielectric behaviour is explained on the basis of Maxwell–Wagner model and Koops phenomenological approach.

Keywords. Higher concentration Cd-doped ZnO alloys; solution method; optical and dielectric studies.

1. Introduction

Compound semiconductors, such as ZnO nanostructures have gained much attention over the past few years in the research community because of their attractive properties. ZnO is easily commercially available, non-toxic, low price and high chemically stable material [1–3]. Scientifically, ZnO is an amphoteric oxide and direct semiconductor material with a large direct band gap ($E_g = 3.2\text{--}3.4$ eV) at 300 K [4–7] which is useful for better optical properties. ZnO also has an exciton binding energy (60 meV) [8] larger than other semiconductor materials, such as ZnSe (21 meV) [9] and GaN (22 meV) [10]. Due to these properties, ZnO has a lot of applications in photovoltaics, optoelectronic devices [11,12], UV-light emitters, transparent conducting films, gas sensors, antibacterial activity, catalyst and surface acoustic wave (SAW) device [13–21], etc. Zn is a member of group-12 in the periodic table and just below the zinc, we have cadmium. From the application point of view, cadmium oxide (CdO) is also a II–VI group n-type semiconductor and exists as a rock salt structure (FCC), which has interesting properties for optoelectronic applications due to its low electrical resistivity, large band gap and high optical transmittance in the visible range of the solar spectrum.

CdO has an optical direct band gap of about 2.2 eV and an indirect band gap of 1.98 eV, which makes it useful for a wide range of applications, such as solar cells, photodiodes and transparent electrodes and sensors, etc. So, one can expect that a composite alloy of Zn and Cd oxides should show magnificent behaviour. Different research groups have tried various methods to prepare the $Zn_{1-x}Cd_xO$ alloy nanostructures, such as sol–gel [22], sonochemical method [17], combustion synthesis [23,24], hydrothermal method [20], solution method [25], etc. In the semiconductor world, doping/alloying (here, alloying means doping with a high percentage) is an efficient means for improving physical properties, especially, optical and electrical ones, or tuning them as per need and applications. Also, to control the band engineering and optoelectronics, usually, semiconductor heterostructures are used to control carrier transport. A literature survey suggests the unusual chemical, structural and physical changes in doped ZnO nanoparticles [24,26]. It has also been pointed out that the doping of Cd into ZnO in the proper amount does not give a significant change in the crystal structure and the lattice constant of ZnO [20]. Besides, doping of Cd^{2+} ions into ZnO lattice gives enlarged conductivity [13] and increases the carrier concentration. Although $Zn_{1-x}Cd_xO$ alloys have been

synthesized in a different structure, such as thin-film [27,28], nanorods [29], nanowires [30], nanosphere [31] and nanoflowers [32]. CdO has a rock salt structure which limits the equilibrium solubility in wurtzite ZnO to a mole fraction of $x = 0.02$, means very little flexibility to tune the properties. Further, there are many reports available in literature related to the structural and optical studies of Cd-doped ZnO nanostructures [17,33–35]. Ghosh *et al* [36] used a high-pressure solution growth method for the synthesis of $Zn_{1-x}Cd_xO$ ($x = 0, 0.021, 0.025, 0.046, 0.091$) nanostructures. They found that cubic phase of CdO was segregated for 9% Cd-doped ZnO sample. Yue Wang *et al* [17] synthesized $Zn_{1-x}Cd_xO$ ($x = 0, 0.05, 0.15, 0.4$) nanoparticles by using sonochemical method. They did not find separate phase of CdO up to 40% of Cd doping. On the basis of above discussed results, it can be inferred that synthesis method strongly affects the structural and optical properties of Cd-doped ZnO nanostructures. Apart from this, literature survey also suggest that there are very few reports related to dielectric study for Cd-doped ZnO nanostructures [37,38]. So, in this work, a different approach was adopted which is also known as chemical solution method for the synthesis of Cd-doped ZnO nanoparticles. Solution method is opted, because this method is at low-temperature, needs simple equipment, low-cost, environment friendly, short annealing time, good control of size and a vast amount of samples can be prepared at a time. In this work, it has also been tried to prepare pure phase different Cd-doping concentrations from 10 to 40% in a sequence order. In addition to structural and optical studies of Cd-doped ZnO nanostructures, dielectric study has also been investigated at room temperature. Different characterization techniques give information that doping of Cd in ZnO nanoparticles is effective to change various structural, optical, and electrical behaviours of ZnO. These changes in optical and dielectric properties are preferred to use Cd-doped ZnO nanoparticles in the field of optoelectronics, photocatalyst, dynamic random-access memory and high-frequency device applications.

2. Experiment

2.1 Chemicals

Zinc acetate ($Zn(CH_3COO)_2 \cdot 2H_2O$) and cadmium nitrate ($Cd(NO_3)_2$) were used as a source of zinc and cadmium, respectively. Apart from these, methanol (CH_3OH) and distilled water were used as solvents. Sodium hydroxide (NaOH) was used for precipitate formation and to maintain the pH of the solution. Finally, ethanol (C_2H_5OH) was used for washing the precipitates. In this experiment, all the chemical reagents were of analytical grade and have been used without any further purification.

2.2 Synthesis of samples

Undoped and Cd-doped ZnO nanoparticles were synthesized by the solution method. An aqueous solution of zinc acetate in methanol (say A) and cadmium nitrate in distilled water (say B) were taken in the stoichiometric ratio in separate beakers and after 5 min, solution A was gradually mixed with solution B. The obtained mixture solution (A+B or say C) was stirred on the magnetic stirrer for getting a homogeneous and clear solution at room temperature. Then, a measured amount of NaOH was added to the above solution C to get pH 9 and obtained a milky white thick solution. This solution was stirred by the magnetic stirrer for 1 h. Later, the obtained solution was centrifuged for 15 min and got white precipitate. In the next step, precipitates were dried in a hot air oven at $90^\circ C$. After drying, the obtained materials were grounded with the help of agate mortar and pestle to obtain a fine powder. Finally, the powder was calcined at $250^\circ C$ for 2 h to get $Zn_{1-x}Cd_xO$ ($x = 0.1, 0.2, 0.3$ and 0.4) nanopowder samples. For pure ZnO synthesis, we followed the above process without taking solution B (cadmium nitrate in distilled water). A similar preparation method is adopted in our previous published work [39].

2.3 Instrumentation

Various experiments were done to characterize the structural, optical and magnetic properties of synthesized samples. The structure analysis of synthesized samples was done by X-ray diffraction (XRD) using XRD-D8 Advance, Bruker diffractometer with $CuK\alpha$ radiation ($\lambda = 0.15418$ nm). To determine surface morphology and to confirm doping, we used SEM and EDX by using FEI Quanta 200 equipped with EDX. In addition to SEM, particle size was analysed by using FEI TECNAI F30 STWIN transmission electron microscope (TEM). The optical properties were examined with UV-Vis and FTIR spectroscopy by using UV-Vis-NIR-Lambda 950, PerkinElmer Spectrophotometer and FTIR-Frontier, PerkinElmer Spectrometer. The room temperature dielectric measurements were investigated by using the impedance analyzer of Wayne Kerr Electronics 6500 B series.

3. Result and discussion

3.1 Structural investigation

Figure 1 depicts the XRD pattern of ZnO and Cd-doped ZnO samples with a different molar concentration of Cd. All peaks in XRD pattern of $Zn_{1-x}Cd_xO$ ($x = 0, 0.1, 0.2, 0.3$ and 0.4) samples were matched with standard International Centre for diffraction data (ICDD files for ZnO, 01-079-0206). From the XRD patterns of $Zn_{1-x}Cd_xO$ ($x = 0, 0.1,$

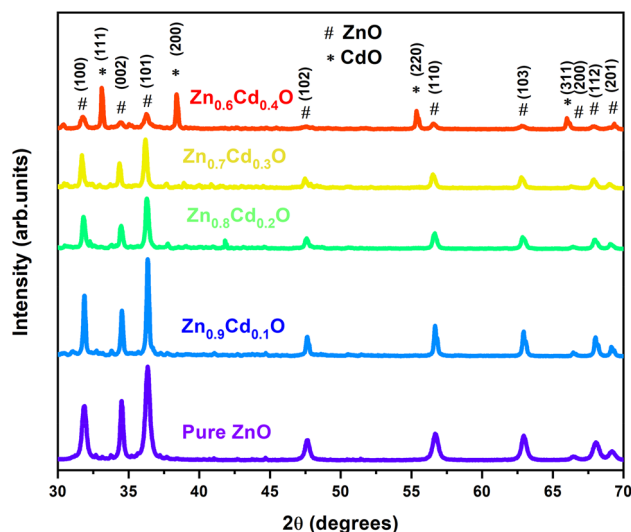


Figure 1. XRD patterns for undoped ZnO and Cd-doped ZnO nanopowders.

0.2, and 0.3), it is clear that as-prepared samples have only wurtzite ZnO phase and no peaks are corresponding to either cadmium, zinc, or their complex oxides within measurable limits of XRD. This shows that $\text{Cd}^{2+}/\text{CdO}$ is dispersed in the matrix of ZnO. It is important to note that because of different crystal structures of ZnO (wurtzite) and CdO (rock salt), they have very little miscibility and tend to get phase-separated easily and the thermodynamic solubility limit of Cd in the ZnO system is around 2 mol% under equilibrium conditions [40]. But the formation of any metastable phase via solution method is controlled by chemical kinetics and thermodynamics involved in the process and, in this condition, the bath condition favour to crystallize single phase. Apart from this, on increasing Cd^{2+} ions concentration (up to $x = 0.3$) into ZnO, there are few visible changes in the diffraction peaks, like a variation in the intensity of the XRD peaks, shifting of XRD peak positions and the broadening of peaks of ZnO. The Cd^{2+} ions that were introduced into ZnO matrix interstitial are responsible for shifting peak positions [41,42]. The presence of Cd^{2+} ions in the ZnO matrix creates micro strain and hence, lattice deformation and this strain effect are reflected in the broadening of full width at half maximum (FWHM) of peaks. Micro strain can be calculated by using the following equation [43]:

$$\varepsilon = \frac{\beta \cos \theta}{4}, \quad (1)$$

where ε is micro strain, β the FWHM and θ the Bragg's angle. It is observed that micro strain is reduced for doped samples. Micro strain values for all samples are shown in table 1.

For $x = 0.4$, Cd-doped ZnO sample, XRD confirms the presence of a combination of two phases, cubic CdO and hexagonal ZnO. This means that both the phases of ZnO and CdO are present as separate entity. Importantly, one of

the basic constraints to make CdO via chemical route is the formation of CdO at relatively high temperatures (230°C) which is the boiling point of most of the organic solvents used for the solution method. Here, for $x = 0.4$, i.e., high concentration of Cd^{2+} ions favour to form CdO as separate phase. Peak position corresponding to CdO is mentioned with an asterisk (*) in the XRD pattern. So, based on the X-ray investigation, we can divide the as-prepared samples into two parts: (i) single-phase Cd-doped ZnO (when Cd doping is up to 30%); where there is no sign of the presence of CdO, and (ii) mixed-phase of ZnO and CdO (when Cd doping is >30%); means binary compositions of semiconductors ZnO–CdO. Broadening in FWHM of a peak shows the formation of the nanostructure. Considering the instrumental broadening, the average crystallite size of ZnO nanoparticles was calculated with the help of XRD peak (101) by using the Scherrer's formula [44,45]

$$D = \frac{0.89\lambda}{\beta \cos \theta}, \quad (2)$$

where D is the average crystallite size, θ the Bragg's angle in radian, λ the incident X-ray wavelength (0.15406 nm) and β the FWHM. The average crystallite size of undoped ZnO was found to be 22 nm and the average size of Cd-doped ZnO was found between 39 and 33 nm (for $x = 0.1, 0.2$ and 0.3). For $x = 0.4$ Cd-doped ZnO, crystallite size, corresponding to ZnO was found to be 23 nm and the crystallite size of CdO was 48 nm. For sample $x = 0.4$, the crystallite size of ZnO is equivalent to pure phase ZnO and may be because of the segregation of CdO from the ZnO matrix, and a similar result is reported by Jule *et al* [13]. The magnified view of diffraction peak (101) is shown in figure 2a for pure ZnO and Cd-doped ZnO samples. From figure 2a, we can easily see the shifting of (101) peak and also see a decrease in the peak intensity of ZnO with increasing molar concentration of Cd^{2+} ions into ZnO lattice. The lattice parameters (a and c) of ZnO wurtzite structure were determined from (100) and (002) diffraction peaks by using the following equations [25]:

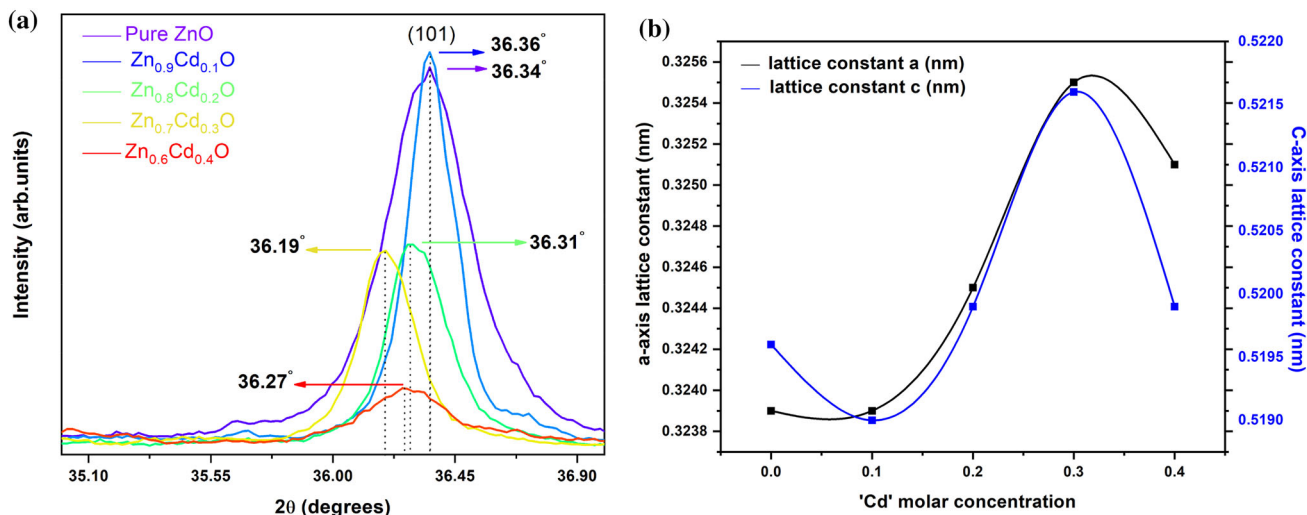
$$a = \frac{\lambda}{\sqrt{3} \sin \theta_{100}}, \quad (3)$$

$$c = \frac{\lambda}{\sin \theta_{002}}, \quad (4)$$

The values of lattice parameters for pure ZnO were found ($a = b = 0.3241$ nm and $c = 0.5199$ nm) and these values are well-matched with the theoretical values of lattice parameters [45]. The value of lattice parameters is increased for Cd-doped samples (for $x = 0.1, 0.2$ and 0.3), it may be because of larger ionic radii of Cd^{2+} ions (0.97 nm) than Zn^{2+} ions (0.74 nm) [13,46]. The variation in lattice parameters a and c are shown in figure 2b for the different molar concentrations of Cd^{2+} ions into the ZnO lattice. At $x = 0.4$, ZnO is tending towards pure phase which is also supported by lattice parameters' calculations. So, $x = 0.4$

Table 1. Calculated lattice parameters (a and c), micro strain and volume of unit cell for pure ZnO and Cd-doped ZnO samples.

Sample	a (nm)	c (nm)	Micro strain (10^{-3})	Volume of unit cell (nm^3)
Pure ZnO	0.3241	0.5199	1.72	0.04729
Zn _{0.9} Cd _{0.1} O	0.3241	0.5196	0.936	0.04726
Zn _{0.8} Cd _{0.2} O	0.3245	0.5202	1.13	0.04743
Zn _{0.7} Cd _{0.3} O	0.3257	0.5219	1.07	0.04794
Zn _{0.6} Cd _{0.4} O	0.3251	0.5205	1.52	0.04764

**Figure 2.** (a) Magnified view of (101) diffraction peak and (b) variation in lattice parameters (a and c) for different molar concentrations of Cd^{2+} ions into ZnO lattice.

sample is pure binary composition of semiconductors ZnO–CdO. The volume of unit cell for all samples was determined by using a formula:

$$V = 0.866a^2c, \quad (5)$$

where V is the volume of a unit cell, a and c are lattice parameters. The volume of the unit cell for doped samples is increased due to the increment in lattice parameters values with Cd doping. The increment in unit cell volume is also confirmed by the successful substitution of Zn^{2+} ions by Cd^{2+} ions. The parameters related to XRD results, such as lattice parameters (a and c), micro strain, volume of a unit cell, etc. are tabulated in table 1.

3.2 Surface/particle morphology analysis

To study the physical appearance and surface topography of as-prepared samples, we took SEM. As a representation, here, we have included two samples. Since the XRD pattern was unable to give any sign for the presence of Cd in the sample (up to $x = 0.3$) and hence, it was necessary to go for elemental analysis and EDX analysis associated with SEM was used. To see the variation of Cd in the samples, EDX

was performed at several places for the same sample and it was found that the sample is inhomogeneous with respect to Cd. The SEM images for pure ZnO and $x = 0.2$ Cd-doped ZnO samples are shown in figure 3a and b, respectively. EDX images are shown in figure 3c and d for pure ZnO and $x = 0.2$ Cd-doped ZnO sample. The SEM micrographs show the effect of Cd doping in ZnO. By comparing figure 3a and b, we can say particles are more agglomerated in the doped samples than undoped ones. ZnO nanoparticles are clustered because of minimization of their surface free energy [46]. The agglomerations of nano-sized particles are very common. The spectrum (figure 3c) for pure ZnO nanopowder sample confirms the existence of zinc and oxygen elements only and EDX spectrum figure (3d) for $x = 0.2$ Cd-doped ZnO sample shows the presence of cadmium, zinc and oxygen elements only. EDX pattern shown in figure 3d confirms the presence of Cd^{2+} ions in the ZnO matrix.

To precisely study the particle size of pure ZnO and $x = 0.2$ Cd-doped ZnO samples, we have done the TEM characterization and corresponding results are presented in figure 4a–d, respectively. Both samples show the formation of nanoparticles with a nearly spherical and hexagonal shape with an average size of 30 nm, which is consistent with the XRD findings.

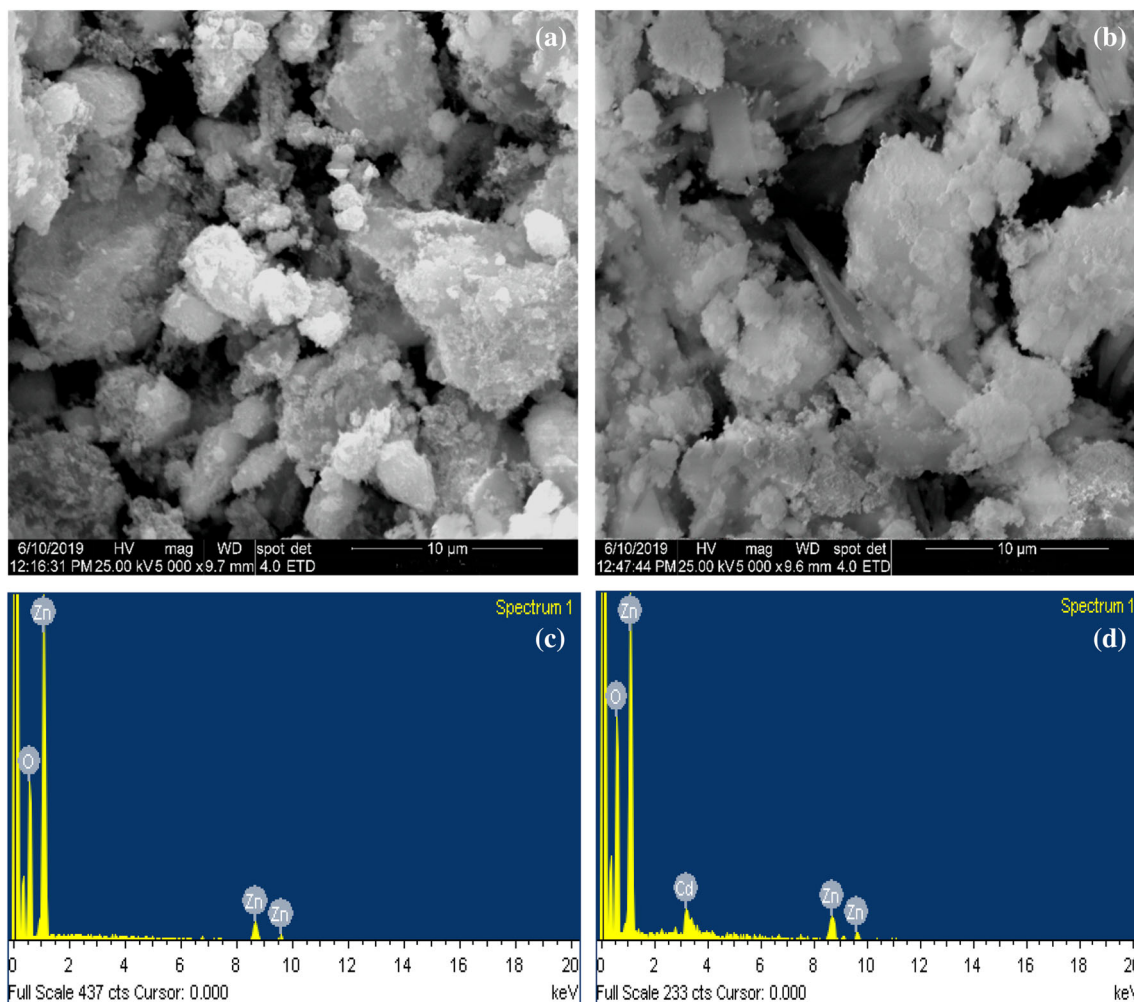


Figure 3. SEM images (a) and (b) and EDX spectrum for pure ZnO nanopowder (c) and (d) and Cd-doped ZnO ($x = 0.2$) nanopowder samples, respectively.

3.3 UV-visible study

Earlier extensive research shows that doping has a strong ability to tune and engineer the optical band gap of ZnO. Cd and Zn are from the same group of the periodic table (group 12) and are transition metals, and hence, it is expected that doping of Cd in ZnO should manifest interesting features in the sample. The absorption spectra for pure and Cd-doped ZnO nanopowders show a strong absorption edge below 400 nm (figure 5). The optical band gap E_g has been calculated by using the Tauc relation [47]. The Tauc relation for semiconductor material is given by the following equation:

$$\alpha hv = A(hv - E_g)^m, \quad (6)$$

where α is the absorption coefficient, ν the incident light frequency, A the proportionality constant, h the Planck's constant, E_g the optical band gap energy and m the 1/2 for direct band gap material [14]. Since ZnO is a direct semiconductor material, a graph $(\alpha hv)^2$ vs. $h\nu$ was plotted for

calculating the optical band gap by using the Tauc relation (equation 6).

Figure 6a–e show Tauc plots between $(\alpha hv)^2$ and $h\nu$ for pure and Cd-doped ZnO samples. For all plots of figure 6a–e, a straight line was fitted for the linear portion of the curve. The extrapolation of the straight line (tangent passing through the point of inflection of the curve) on the x -axis (E_g axis) gives the energy band gap value. The band gap was found to be 3.17 eV for pure ZnO sample and 3.09, 3.05, 3.0 and 2.72 eV for $x = 0.1, 0.2, 0.3$ and 0.4 samples, respectively. The band gap variation for ZnO with Cd molar concentration is shown in figure 7. This low value of 3.17 eV of the band gap for pure ZnO is similar as reported in the literature [14]. Band gap value decreases from 3.17 to 2.72 eV as Cd-doping concentration amount increase up to $x = 0.4$. Similar observations were reported by [13] for Cd-doped ZnO alloys synthesized via the sol-gel route. This redshift in the band gap of ZnO is because of changes in the electronic structure of ZnO by Cd doping. This leads to reducing the ionic character of Zn–O/Cd–O on the

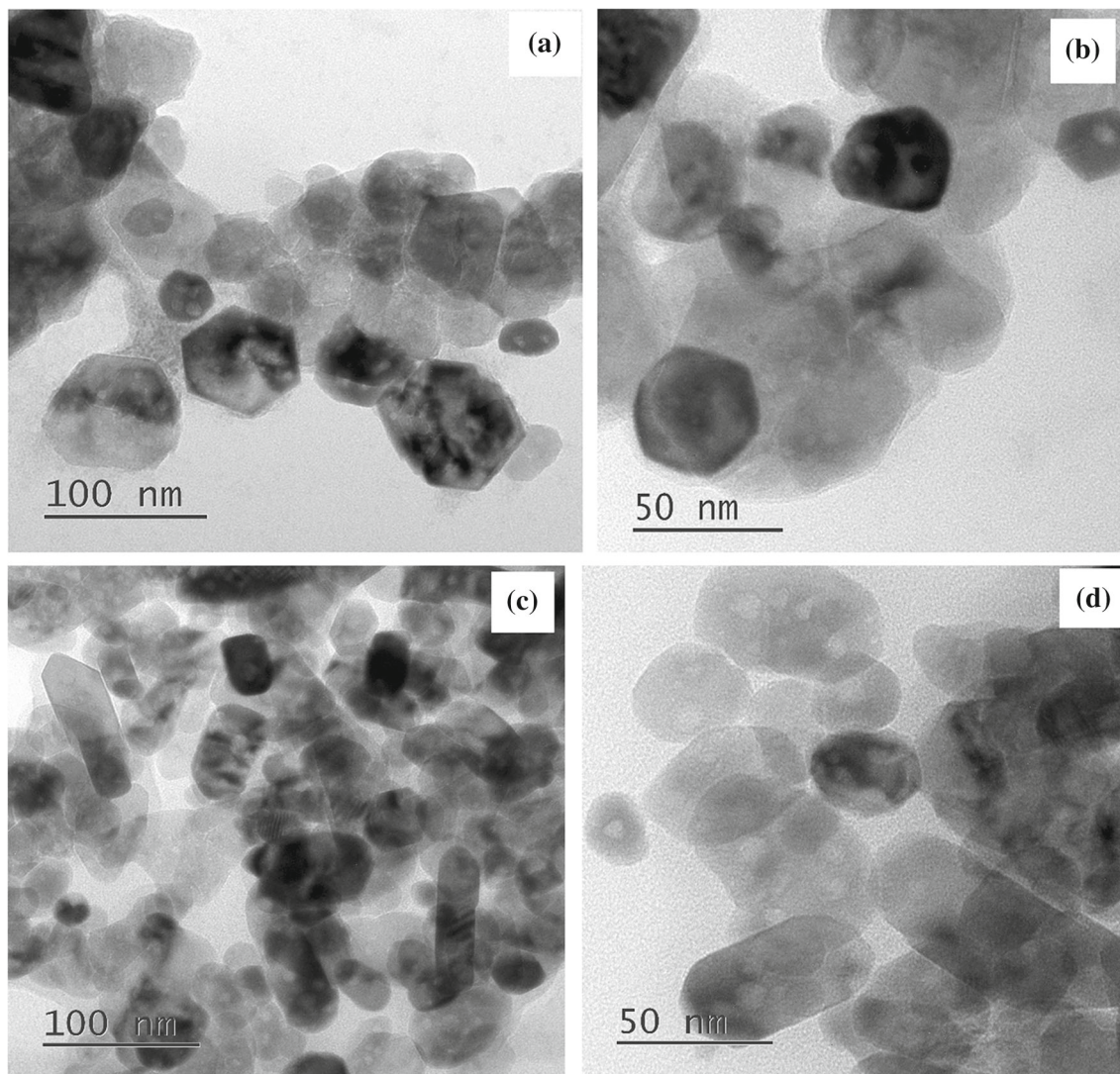


Figure 4. TEM micrographs for (a) and (b) pure ZnO and (c) and (d) Cd-doped ZnO ($x = 0.2$) sample.

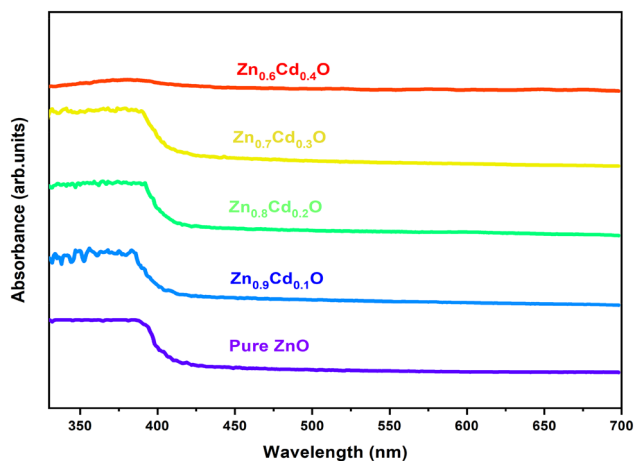


Figure 5. UV-visible absorption spectra of undoped ZnO and Cd-doped ZnO nanopowders.

substitution of Zn^{2+} ions by Cd^{2+} ions. Moreover, Jule *et al* [13] reported that the conduction band of ZnO consists of Zn 4s and O 2p orbitals, of which Zn 4s orbital is dominated. But due to the incorporation of Cd into ZnO, Cd 5s state also contributes to the conduction band of ZnO with Zn 4s state, this leads to the shifting of the conduction band downwards and hence, band gap of ZnO becomes narrow with Cd doping. Therefore, Cd-doped ZnO nanostructures can be used for small band gap applications.

3.4 FTIR analysis

Figure 8 depicts the FTIR spectrum for pure ZnO and doped ZnO samples in the range of $400\text{--}4000\text{ cm}^{-1}$. The range from $4000\text{ to }1800\text{ cm}^{-1}$ is called the functional group region and $1800\text{--}400\text{ cm}^{-1}$ is the fingerprint region for a

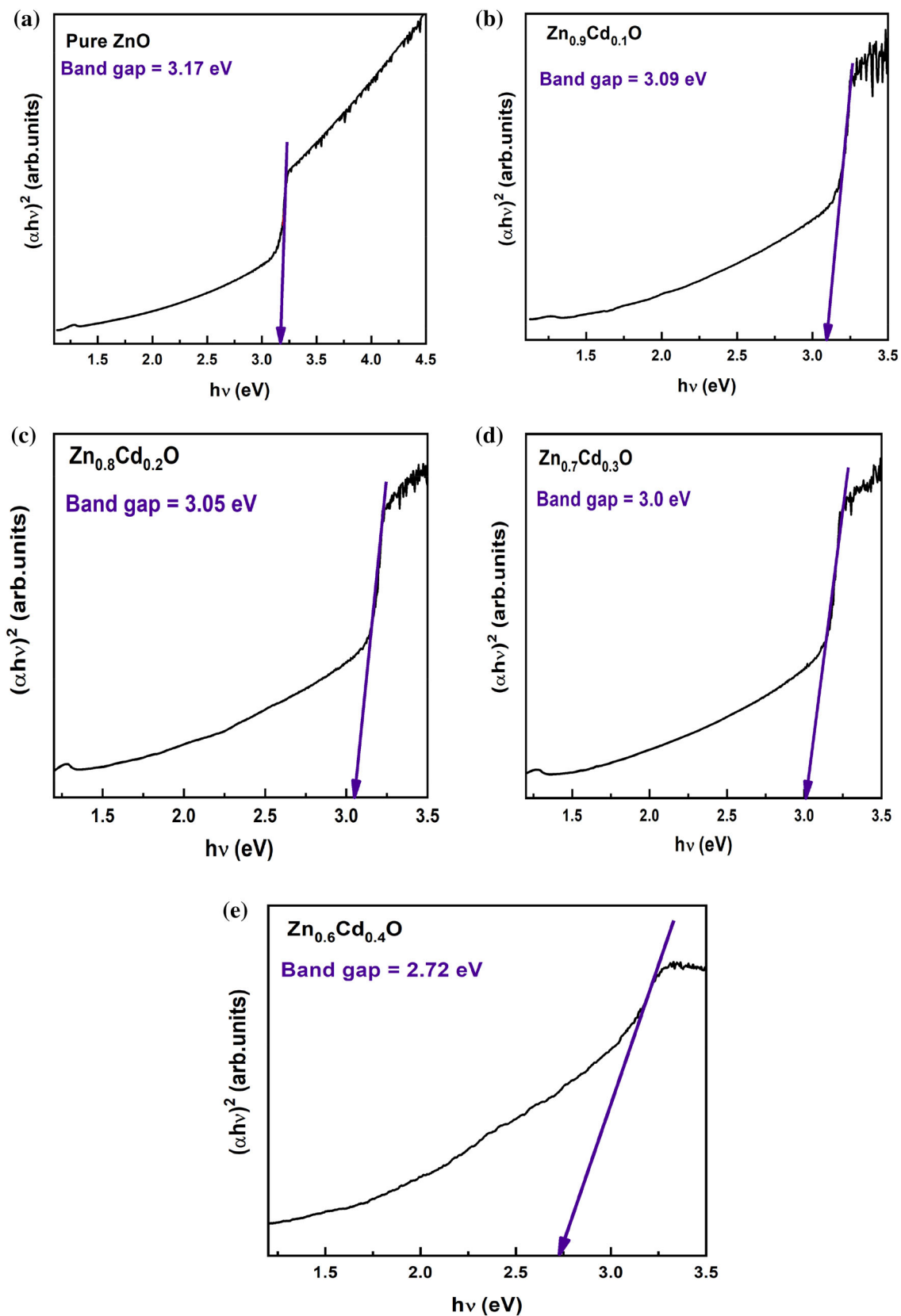


Figure 6. Tauc's plots for pure ZnO and Cd-doped ZnO samples.

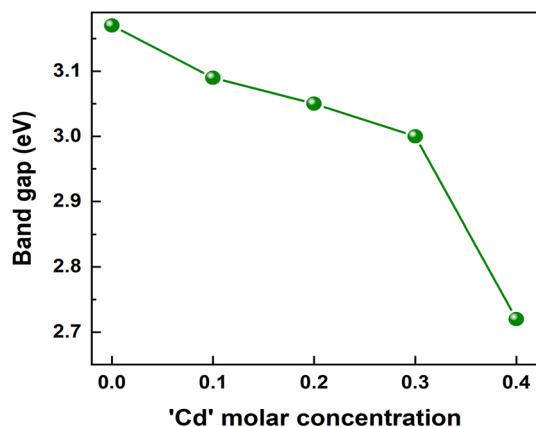


Figure 7. Band gap variation in ZnO with dopant molar concentration.

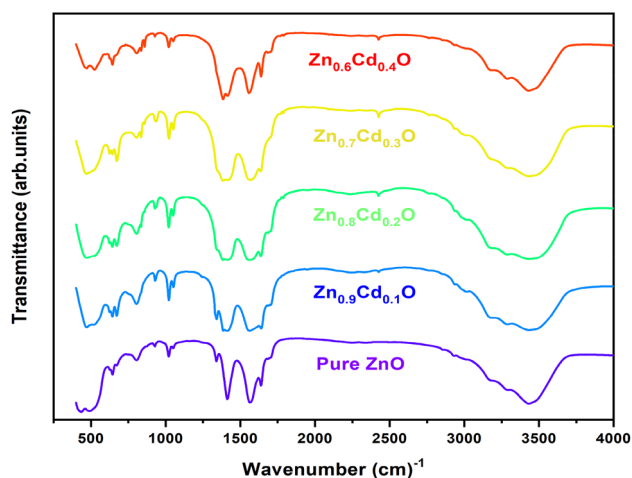


Figure 8. FTIR spectra for pure ZnO and Cd-doped ZnO for different concentrations of dopant.

material. FTIR study was carried out for confirmation of wurtzite structure formation and to get information about functional groups for undoped and Cd-doped ZnO alloys. Metal oxides generally give absorption bands below 1000 cm^{-1} emerging from inter-atomic vibrations. The absorption peak in the range from 1000 to 3500 cm^{-1} belongs to impurities vibration modes. The absorption peak nearly at 3425 cm^{-1} , corresponds to O–H stretching vibration that indicates the existence of atmospheric water adsorbed on the surface of samples. This O–H group plays an important role in the performance of a material as a photocatalyst due to the high oxidizing nature of this group [48]. The absorption band around 2926 cm^{-1} belongs to vibrations of C–H stretching for an alkane. A dip has been observed around 2421 cm^{-1} which arises due to the absorption of atmospheric CO_2 on the surface of metal cations [42]. Peaks at 1643 and 1409 cm^{-1} correspond to C=C and C–C stretchings, respectively. The carboxyl group (CO) vibrations belong to the region 1500 – 1600 cm^{-1} . The Cd=O stretching vibration was observed nearly at 1379 cm^{-1} for

doped ZnO samples. The absorption peaks near to 812 and 1023 cm^{-1} correspond to C–OH stretching. The wurtzite Zn–O stretching vibration modes reside in the region of 400 – 600 cm^{-1} [49]. We found an absorption peak for pure ZnO at 435 cm^{-1} and Cd-doped ZnO samples nearly at 465 cm^{-1} , these absorption peaks confirm the stretching vibration modes of Zn–O. The prepared samples can be used as a photocatalyst due to the presence of a highly oxidizing O–H group.

3.5 Electrical characterization

To study the electrical response for the prepared samples, the external electrical field has been applied to investigate the interaction between the electric field and material. This interaction has been studied using an impedance analyzer.

3.5a Dielectric study: Dielectric properties for the prepared samples have been studied as a function of the frequency of the applied electric field. For the dielectric study of synthesized nanopowders, disc shaped pellets were formed from nanopowders by applying 10 kN force for 3 min using a universal testing machine (UTM). The diameter and thickness of these pellets were 16 and 3 mm , respectively. The pellets were further coated with high purity silver paste on parallel faces as the electrodes to make the parallel plate capacitor geometry.

The relative dielectric constant as a complex quantity can be written as [50]:

$$\varepsilon^* = \varepsilon' + j\varepsilon'' \quad (7)$$

where ε' (real part) represents stored energy and ε'' (imaginary part) describes energy loss in a dielectric material during the polarization in applying the electric field.

To understand the effect of Cd doping on the electrical behaviour of ZnO, the frequency-dependent real dielectric constant (ε') for these Cd-doped ZnO samples were measured using the following equation [50],

$$\varepsilon' = C_p t / \varepsilon_0 A, \quad (8)$$

where C_p is the capacitance of pellet in Farad (F), t the thickness of pellet, ε_0 ($\varepsilon_0 = 8.85 \times 10^{-12}\text{ F m}^{-1}$) permittivity of free space and A the cross-sectional area of the flat surface of the pellet.

The imaginary part (ε'') can be estimated by using the following relation [51]:

$$\varepsilon'' = \varepsilon' \tan \delta, \quad (9)$$

where $\tan \delta$ is dielectric loss tangent for a dielectric material. It is proportional to energy loss, dissipated in the form of heat during the polarization of dielectric material therefore, it is called dielectric loss.

The variation in dielectric constant with frequency (frequency range from 20 Hz to 1 MHz) is shown in figure 9. This showed a rapid decrease in dielectric constant value at

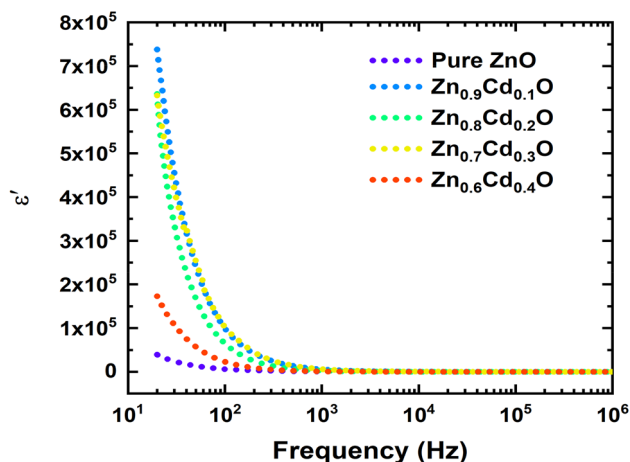


Figure 9. Variation in dielectric constant with frequency for pure ZnO and Cd-doped ZnO nanopowder samples.

lower frequencies, while at higher frequencies, dielectric constant became almost independent of frequencies for all samples. This type of dielectric behaviour for ZnO and ZnO-related nanostructures is available in the literature [52]. And this dielectric nature can be explained by the Maxwell–Wagner interfacial model [53] and Koops phenomenological theory [54]. It is accepted that dielectric materials are comprised of well-conducting grains which are separated by less conduction grain boundaries, these grain boundaries behave as a potential barrier for charge carriers [55]. Grain boundaries are more effective at lower frequencies, while grains are more competent at higher frequencies. When these dielectric materials are placed in an external electric field, charge carriers smoothly move within the grain, but accumulated at grain boundaries therefore, interfacial polarization is produced [56,57]. This behaviour of charge carriers inside dielectric materials can form large polarization so, the high dielectric constant is found at lower frequencies. Dielectric constant decreases as frequency increases because any species which is responsible for polarizability is found to express as lagging behind the applied electric field at very high frequencies [53]. Frequency-independent dielectric behaviour at higher frequencies was because of dipoles that are unable to follow the applied external electric field beyond a certain frequency. In figure 9, the pure ZnO sample shows the lowest value of dielectric constant, while the dielectric constant value increased in doped samples. These increments in the doped samples may be due to an increase in charge carrier concentration in Cd-doped ZnO samples. Since the dielectric polarizability of Cd ions is more than Zn ions [58], so as the doping concentration increases, more Zn ions will be substituted by Cd ions. It increases the dielectric polarization, and hence, more dielectric constants have been found for doped samples. Importantly, $x = 0.4$ in figure 9 shows the low value of dielectric constant (but more than pure ZnO), this is because $x = 0.4$ is a mixed phase of ZnO and CdO (binary composition of semiconductors ZnO–CdO).

For this sample, the low value of dielectric constant also reveals that there is little or no doping of Cd in ZnO or Zn in CdO for this sample means both ZnO and CdO are in an almost pure phase. This observation is in favour of the X-ray result. 10% Cd-doped ZnO showed a higher dielectric constant among all doped samples. So, $x = 0.1$ is the most appropriate concentration among the elaborated series for Cd doping into ZnO.

3.5b Dielectric loss: In a real sense, on this earth, there is no lossless material as such. All materials are lossy except the perfect vacuum (which we cannot attain). Now, the degree of the loss will decide/distinguish the quality of material and its usability/applicability and so, a dielectric loss study was performed for as-prepared materials. Dielectric loss or loss tangent ($\tan \delta = \epsilon''/\epsilon'$) is described as energy loss in a dielectric material. Variation in $\tan \delta$ with frequency is shown in figure 10 for all the prepared samples. All samples showed a relaxation peak which appeared at low frequency for pure ZnO, while for doped samples, it was shifted towards higher frequencies. The shifting in the relaxation peak of dielectric loss for doped samples may be because of Cd doping into ZnO. The observed peak in the dielectric loss is because of the resonance effect. When the jumping frequency of charge carriers is equal to the frequency of the applied field and the condition $\omega\tau = 1$ ($\omega = 2\pi n$; n = frequency), is satisfied then, this kind of loss peaks occurs. When the frequency of the applied electric field matches with the hopping frequency of the charge carrier, the maximum electrical energy is transferred to the oscillating ions and a peak is observed as a result of power loss [59]. Among all samples, 10 and 30% Cd-doped ZnO sample show appropriate values of dielectric constant and dielectric loss. So, these samples can be used for device applications [53].

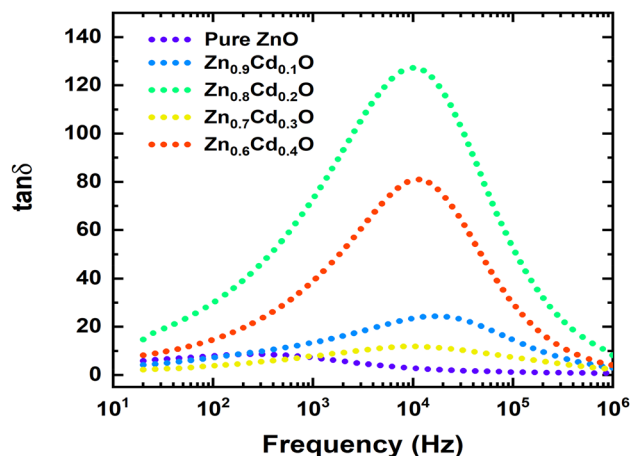


Figure 10. Variation in tangent loss with frequency for pure ZnO and Cd-doped ZnO nanopowder samples.

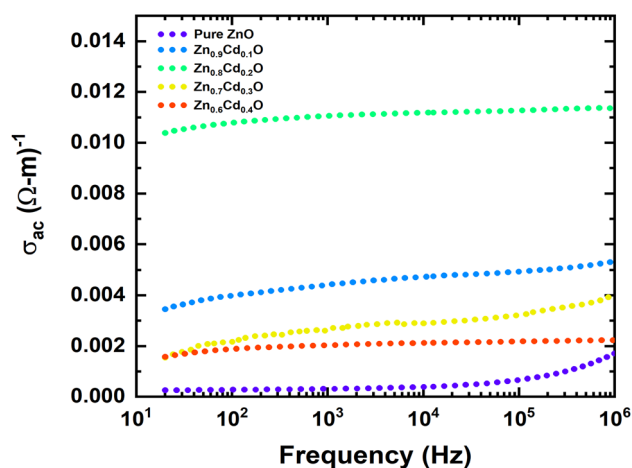


Figure 11. Variation in ac conductivity with frequency for pure ZnO and Cd-doped ZnO nanopowder samples.

3.5c *ac electrical conductivity*: ac conductivity for all the prepared nanopowder samples was estimated by using the following empirical relation [60]:

$$\sigma_{ac} = \omega \epsilon' \epsilon_0 \tan \delta, \quad (10)$$

where σ_{ac} is AC electrical conductivity and $\omega = 2\pi f$ (f being the frequency) is the angular frequency. σ_{ac} was estimated in the frequency range of 20 Hz to 1 MHz at room temperature and variation in σ_{ac} with frequency is shown in figure 11. From figure 11, it is clear that σ_{ac} increased by a large amount for Cd-doped sample as compared to the pure ZnO sample. σ_{ac} gradually increased as frequency increased for all samples. This gradual increase in σ_{ac} with frequency shows enhancement in the movement of charge carriers with frequency. The variation in σ_{ac} for pure ZnO sample is very small up to a certain high frequency, beyond this frequency, increment in σ_{ac} is visible. But for Cd-doped samples, σ_{ac} gradually increased as frequency is increased and this increment is also very less. We can say σ_{ac} becomes almost independent at higher frequencies for doped samples, while for pure ZnO sample, it is nearly independent at lower frequencies. The reason behind increasing σ_{ac} for Cd-doped samples may be because of the increase in charge carriers inside the samples due to the Cd dopant. This behaviour can be explained by the hopping model. Increasing σ_{ac} for doped samples is because of the hopping of charge carriers which contain positive oxygen vacancies (V_o^{2+}), zinc interstitials (Zn_i^+), and negative oxygen ions (O^{2-}) that lead to the polarization of ZnO [60]. At higher frequencies, the hopping process increases hence, σ_{ac} increases at higher frequencies. The exchange of charge carriers through hopping between Zn^{2+}/Cd^{2+} ions is responsible for increasing mobility of charge carriers as a result, σ_{ac} is increased [61]. Again, doping at 40% i.e., $x = 0.4$ showed the low value of σ_{ac} (but more than pure ZnO), this is because $x = 0.4$ is a mixed phase of ZnO and CdO, and also reveals that there is little or no doping of Cd in

ZnO or Zn in CdO for this sample means both ZnO and CdO are in almost in pure phase.

4. Conclusion

ZnO and CdO are an immiscible system for higher doping (miscibility, Cd only 2% molar), but here, we report the formation of highly doped $Zn_{1-x}Cd_xO$ ($x = 0.1, 0.2$ and 0.3) alloys in single wurtzite phase with an easy and cost-effective solution method. The solution method is able to maintain the crystal structure of ZnO up to 30% of Cd doping. At $x = 0.4$, the phase CdO is segregated out from ZnO and this is a mixed-phase of ZnO and CdO. The XRD and FTIR observations confirm the formation of the wurtzite structure of ZnO with Cd^{2+} ions doping. FTIR results also show the presence of hydroxyl group for all the prepared samples which is useful as photocatalytic application point of view. TEM micrographs show the formation of nanoparticles for pure ZnO and Cd-doped ZnO samples with an average particle show that the clustering increases with increasing Cd concentration in ZnO. The EDX spectrum confirms the presence of Cd^{2+} ions in ZnO lattice. Tauc plots show redshift in band gap for $Zn_{1-x}Cd_xO$ ($x = 0.1, 0.2, 0.3$ and 0.4) than pure ZnO sample. UV-Vis findings indicate that the Cd doping into ZnO may effectively alter and tune the band gap of ZnO. UV results also suggest that Cd-doped ZnO nanostructures can be used for small band gap applications. The dielectric measurements show that dielectric constant and conductivity are increased in large amount for Cd-doped samples as compared to pure ZnO sample. The dielectric results also confirm that optimal Cd concentration into ZnO leads to high dielectric constant, low tangent loss and high conductivity for microwave and radio frequency applications.

Acknowledgement

We acknowledge Dr Pramod Chaitanya, St. Aloysius College, Jabalpur, India, for going through this manuscript.

References

- [1] Kim H, Piqué A, Horwitz J S, Murata H, Kafafi Z H, Gilmore C M *et al* 2000 *Thin Solid Films* **377** 798
- [2] Subramanyam T K, Srinivasulu Naidu B and Uthanna S 1999 *Opt. Mater. (Amst.)* **13** 239
- [3] Li X F, Cao Y, Sui Y R, Yang J H, Yue Y G, Zhang Q *et al* 2014 *Superlattices Microstruct.* **69** 187
- [4] Khorsand Zak A, Abd Majid W H, Abrishami M E and Yousefi R 2011 *Solid State Sci.* **13** 251
- [5] Reddy C V, Babu B and Shim J 2018 *J. Phys Chem. Solids* **112** 20

- [6] Al-Gaashani R, Radiman S, Daud A R, Tabet N and Al-Douri Y 2013 *Ceram. Int.* **39** 2283
- [7] Nirmala M and Anukaliani A 2011 *Physica B Condens. Matter* **406** 911
- [8] Isik M and Gasanly N M 2019 *Mater. Sci. Semicond. Process.* **100** 29
- [9] Sun C, Gu Y, Wen W and Zhao L 2018 *Opt. Mater. (Amst.)* **81** 12
- [10] Shan W, Little B D, Fischer A J, Song J J, Goldenberg B, Perry W G *et al* 1996 *Phys. Rev. B* **54** 16369
- [11] Saboor A, Shah S M and Hussain H 2019 *Mater. Sci. Semicond. Process.* **93** 215
- [12] Kokate S K, Supekar A T, Baviskar P K, Palve B M, Jadhav S R, Mohite K C *et al* 2018 *Mater. Sci. Semicond. Process.* **80** 179
- [13] Jule L T, Dejene F B, Ali A G, Roro K T, Hegazy A, Allam N K *et al* 2016 *J. Alloys Compd.* **687** 920
- [14] Rana N, Chand S and Gathania A K 2015 *Ceram. Int.* **41** 12032
- [15] Mahmoud W E, Al-Ghamdi A A, Al-Heniti S and Al-Ameer S 2010 *J. Alloys Compd.* **491** 742
- [16] Karimi M, Jahangir V, Ezzati M, Saydi J and Behtaj Lejbini M 2014 *Opt. Mater. (Amst.)* **36** 697
- [17] Wang Y, Yang Y, Zhang X, Liu X and Nakamura A 2012 *Cryst EngComm* **14** 240
- [18] Mohan Kumar T, Shekharam T and Nagabhushanam M 2016 *Mater. Today Proc.* **3** 3621
- [19] Basith N M, Vijaya J J, Kennedy L J, Bououdina M, Jenefar S and Kaviyaranan V 2014 *J. Mater. Sci. Technol.* **30** 1108
- [20] Karunakaran C, Vijayabalan A and Manikandan G 2012 *Superlattices Microstruct.* **51** 443
- [21] Padmavathy V and Sankar S 2019 *Superlattices Microstruct.* **128** 127
- [22] Azam A, Ahmed F, Arshi N, Chaman M and Naqvi A H 2010 *J. Alloys Compd.* **496** 399
- [23] Reddy A J, Kokila M K, Nagabhushana H, Chakradhar R P S, Shivakumara C, Rao J L *et al* 2011 *J. Alloys Compd.* **509** 5349
- [24] Rasouli S and Moeen S J 2011 *J. Alloys Compd.* **509** 1915
- [25] Alizadeh E and Baseri H 2018 *Solid State Sci.* **78** 86
- [26] Sagar R V and Buddhudu S 2010 *Spectrochim Acta Part A: Mol. Biomol. Spectrosc.* **75** 1218
- [27] Makino T, Segawa Y, Kawasaki M, Ohtomo A, Shiroki R, Tamura K *et al* 2001 *Appl. Phys. Lett.* **78** 1237
- [28] Mahmoud W E and Al-Ghamdi A A 2010 *Opt. Laser Technol.* **42** 1134
- [29] Sun C W, Xin P, Ma C Y, Liu Z W, Zhang Q Y, Wang Y Q *et al* 2006 *Appl. Phys. Lett.* **89** 181923
- [30] Wang F, He H, Ye Z, Zhu L, Tang H and Zhang Y 2005 *J. Phys. D: Appl. Phys.* **38** 2919
- [31] Li G, Wang X, Wang Y, Shi X, Yao N and Zhang B 2008 *Physica E Low-dimens. Syst. Nanostruct.* **40** 2649
- [32] Liu J Z, Yan P X, Yue G H, Chang J B, Zhuo R F and Qu D M 2006 *Mater. Lett.* **60** 3122
- [33] Peng Y, Qin S, Wang W S and Xu A W 2013 *Cryst EngComm* **15** 6518
- [34] Najim J A and Rozaq J M 2013 *Int. Lett. Chem. Phys. Astron.* **15** 137
- [35] Sui Y R, Cao Y, Li X F, Yue Y G, Yao B, Li X Y *et al* 2015 *Ceram. Int.* **41** 587
- [36] Ghosh M and Raychaudhuri A K 2007 *Nanotechnology* **18** 115618
- [37] Saravanan R, Prakash T, Gupta V K and Stephen A 2014 *J. Mol. Liq.* **193** 160
- [38] Saxena P, Choudhary P, Yadav A, Dewangan B, Rai V N and Mishra A 2020 *Appl. Phys. A: Mater. Sci. Process.* **126** 1
- [39] Singh G P, Aman A K, Singh R K and Roy M K 2020 *Optik (Stuttg.)* **203** 163966
- [40] Haloui A, Feutelais Y and Legendre B 1997 *J. Alloys Compd.* **260** 179
- [41] Franco A, Pessoni H V S and Soares M P 2014 *J. Magn. Magn. Mater.* **355** 325
- [42] Najafi M and Haratizadeh H 2015 *Solid State Sci.* **41** 48
- [43] Singh R, Verma K, Patyal A, Sharma I, Barman P B and Sharma D 2019 *Solid State Sci.* **89** 1
- [44] Shinde K P, Pawar R C, Sinha B B, Kim H S, Oh S S and Chung K C 2014 *Ceram. Int.* **40** 16799
- [45] Mondal A, Giri N, Sarkar S, Majumdar S and Ray R 2019 *Mater. Sci. Semicond. Process.* **91** 333
- [46] Curcio A L, Martínez Espinosa J W, Pizani P S and De Giovanni Rodrigues A 2019 *Opt. Mater. (Amst.)* **89** 344
- [47] El Ghoul J, Barthou C and El Mir L 2012 *Superlattices Microstruct.* **51** 942
- [48] Reddy C V, Babu B and Shim J 2018 *J. Phys. Chem. Solids* **112** 20
- [49] Andrade Neto N F, Matsui K N, Paskocimas C A, Bomio M R D and Motta F V 2019 *Mater. Sci. Semicond. Process.* **93** 123
- [50] Mehedi Hassan M, Ahmed A S, Chaman M, Khan W, Naqvi A H and Azam A 2012 *Mater. Res. Bull.* **47** 3952
- [51] Alghunaim N S and Alhusaiki-Alghamdi H M 2019 *Phys. B Condens. Matter* **560** 185
- [52] Belkhaoui C, Mzabi N and Smaoui H 2019 *Mater. Res. Bull.* **111** 70
- [53] Prodromakis T and Papavassiliou C 2009 *Appl. Surf. Sci.* **255** 6989
- [54] Koops C G 1951 *Phys. Rev.* **83** 121
- [55] Zamiri R, Kaushal A, Rebelo A and Ferreira J M F 2014 *Ceram. Int.* **40** 1635
- [56] Ashok kumar M and Muthukumaran S 2014 *Powder Technol.* **268** 80
- [57] Ashok kumar M and Muthukumaran S 2015 *J. Lumin.* **162** 97
- [58] Reshetnikov N, Curtis L J, Brown M S and Irving R E 2007 *Phys. Scr.* **77** 15301
- [59] Varshney D, Verma K and Dwivedi S 2015 *Optik (Stuttg.)* **126** 4232
- [60] Khera S and Chand P 2019 *Chin. J. Phys.* **57** 28
- [61] Khan R, Zulfiqar, de Araujo C I L, Khan T, Khattak S A, Ahmed E *et al* 2019 *J. Mater. Sci. Mater. Electron.* **30** 3396